A scalable, Rotating Disc Bioelectrochemical Reactor (RDBER) suitable for the cultivation of both cathodic and anodic biofilms

Max Hackbarth [a], Johannes Gescher [b, c, d], Harald Horn [a, e], Johannes Eberhard Reiner [a].

[a] Engler-Bunte-Institut, Water Chemistry and Water Technology, Karlsruhe Institute of Technology (KIT), Engler-Bunte-Ring 9a, 76131 Karlsruhe, Germany

[b] Karlsruhe Institute of Technology (KIT), Institute for Applied Biosciences (IAB), Fritz-Haber-Weg 2, 76131, Karlsruhe, Germany

[c] Karlsruhe Institute of Technology (KIT), Institute for Biological Interfaces (IBG 1), Hermann-von-Helmholtz-Platz 1, 76344 Eggenstein-Leopoldshafen, Germany

[d] Hamburg University of Technology, Institute of Technical Microbiology, Kasernenstraße 12, 21073 Hamburg, Germany

[e] DVGW Research Centre, Water Chemistry and Water Technology, Engler-Bunte-Ring 9a, 76131 Karlsruhe, Germany

Highlights:

- **Construction of a 10 L membrane-less, pressurizable bioelectrochemical reactor**
- **Rotating working electrodes with up to 1 m^2 electrode surface**
- **Electroautotrophic cultivation and quantification of *K. spormannii* biofilms**
- **Initial cell density crucial for successful *K. spormannii* biofilm formation**
- **Anodic operation as MEC with *Shewanella* / *Geobacter* coculture**

Graphical Abstract

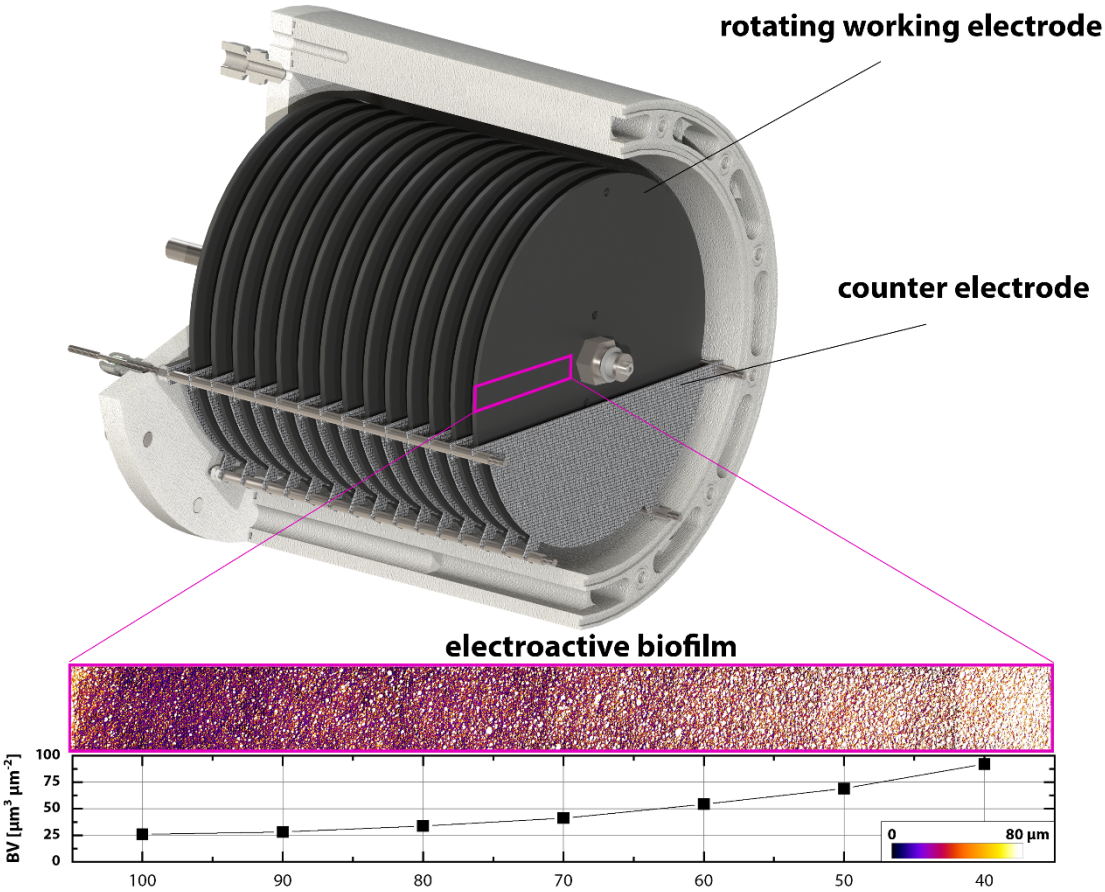

Abstract

The question of whether microbial electrochemical technologies can carve a niche in a future sustainable economy will strongly depend on the availability of suitable reactor technology. However, examples of new, scalable reactor concepts or even scale-ups specifically for microbial electrosynthesis applications are rarely described in the literature. Here, we present a membrane-less reactor system suitable for different bioelectrochemical applications. The system employs rotating graphite disks with a diameter of 210 mm as working electrodes with a total surface area of 1 m^2. Given the reactor volume of 10 L, this results in a surface-to-volume ratio of 100:1 m^2 m^{-3}. Moreover, this rotating disk bioelectrochemical reactor (RDBER) is fully autoclavable, pressurizable to at least 0.5 bars and an optical window allows for the in vivo observation of biofilm development on the electrodes by means of optical coherence tomography (OCT). As a proof-of-principle for an aerobic microbial electrosynthesis process, we cultivated the thermoacidophilic, electroautotrophic bacterium *Kyrpidia spormannii* in the RDBER and investigated the spatial distribution of the cathodic biofilm on the rotating working

electrode by OCT. Thereby, biofilm heights of more than 75 µm were achieved. The initial cell density seems to be crucial for successful *K. spormannii* biofilm formation. To demonstrate the versatility of the system, we further operated the reactor anodically as a microbial electrolysis cell. For this purpose, we inoculated the RDBER with a co-culture of *Shewanella oneidensis* and *Geobacter sulfurreducens* in acetate- and lactate-containing medium at a working electrode potential of 0 mV vs. SHE. During this anodic batch operation, current densities of up to 130 µA cm^{-2} could be achieved. Furthermore, a correlation between the biofilm accumulation rate, current density and hydrogen production as well as substrate degradation rate was observed. These cultivation experiments with different electroactive microorganisms not only prove the basic functionality of the RDBER, but also illustrate that the RDBER can satisfy a wide range of biotechnological requirements for pure culture applications.

1. Introduction

Tapering off fossil resources by renewable commodities that are based on a circular utilization of resources is key to the transition towards a sustainable economy [1]. In this context, future (bio)chemical transformations of raw materials and waste streams must be fueled by renewable electrical energy [2]. The so-called microbial electrosynthesis (MES) is a promising biotechnological example for such a conversion of electricity and carbon dioxide into value-added organic compounds [3]. This process relies on electroactive microorganisms that serve as a biocatalyst on the cathode of a bioelectrochemical system (BES) [4]. By applying a voltage to the BES, typically water is oxidized at the anode into oxygen and protons. Driven by a power source the released electrons are subsequently used either directly or indirectly by the autotrophic, cathodic biofilm as the sole energy and electron source for the reduction of CO_2. Although MES could theoretically outperform abiotic carbon utilization technologies as well as established gas fermentations in some specific applications, the technology is not yet economically feasible on a large scale [5–9]. However, the novel electroautotrophic species *Kyrpidia spormannii* EA-1^T was isolated from a thermophilic cathodic community recently [10]. This thermoacidophilic 'Knallgas' bacterium is a natural producer of polyhydroxyalkanoates (PHAs) and was shown to thrive on cathodes as the sole electron and energy source for the reduction of CO_2 [11]. Hence, *K. spormannii* is a promising candidate for MES - not only since PHAs are precursors for biodegradable bioplastics - but also due to the organisms comparably good biofilm-formation abilities on cathodes. Thus, it was shown that *K. spormannii* forms robust biofilms with a thickness of well over 100 µm – an important prerequisite for MES as stated recently by Vassilev and colleagues [12–14]. Although it seems to be an intrinsic property of electroautotrophic organisms, the molecular details of extracellular electron uptake

(EET) from a cathode are also subject to keen debate with regard to *K. spormannii* [8,11,15,16].

While - with respect to the inanimate components of a MES system - much effort has been put into studying the effect of material and structural properties of electrodes, the development of new and, in particular, scalable reactor concepts for MES has been rather sidelined [15,17–21]. This is in spite of the fact that whether microbial electrochemical technologies (METs) can carve a niche in a future sustainable economy depends strongly on the availability of a suitable reactor technology. Typical reactor systems for the cultivation of electroactive microorganisms in laboratory settings are cube, bottle, or flat-plate-type reactors [22,23]. Especially for MES applications, a semipermeable membrane is commonly required to spatially separate anode and cathode compartments. Membranes can be advantageous when extremely high Coulombic efficiencies are desired, as they avoid chemical short circuits caused by diffusion of electrochemically active chemicals [22]. Moreover, due to anodically produced oxygen a membrane is particularly crucial if strict anaerobes, such as acetogenic or methanogenic organisms, serve as cathodic biocatalysts for MES [24]. However, the utilization of membranes leads to significantly increased surface-specific ohmic losses as a plain result of an increased distance between anode and cathode, but also through diffusion limitations often caused by hardly mixed zones around the membranes. The latter may also result in undesirable pH shifts in the separated compartments [8,22,24–26]. Finally, most membranes are not autoclavable (according to the manufacturer), sensitive to fouling and prone to leakage due to lack of mechanical stability [27]. The above-mentioned disadvantages of membranes, along with the resulting complexity of the reactor set-up, lead to a high-maintenance reactor system which is likely to be very cost-intensive in long-term operation [28].

Here, we present the concept of a membrane-less, scalable rotating disk bioelectrochemical reactor (RDBER) for aerobic MES and other pure culture bioelectrochemical applications. The systems design is inspired by a so-called rotating biological contactor (RBC) [29]. An RBC is a fixed-film bioreactor used in wastewater treatment that consists of closely spaced discs that are mounted on a common horizontal shaft and are typically partially submerged in liquid. Cortez and colleagues highlight the low maintenance and operating costs, ease of process control and monitoring, and low land requirements as particular advantages of an RBC [30]. This is mainly due to the fact that the flow velocity across the biofilm enhancing substrate supply is not achieved by energy-intensive pumping of high volumes or stirring, but by rotation of the biofilm-covered disks. The first steps in the "electrification" of RDCs have already been successfully carried out on a laboratory scale [31–34]: Several attempts have been made to use conductive rotating disks as cathode or anode of a bioelectrochemical system. However, these studies consistently focus on the purification of wastewater. Hence, biotechnological requirements for a pure culture MES process (e.g., working with pure cultures under sterile

121 conditions, control of temperature and pH, or pressurizability to increase the solubility of the
122 gaseous substrates like CO_2) were not considered in the reactor design.

123 In this study we discuss the development of a fully autoclavable RDBER, that can be
124 pressurized to at least 0.5 bar, and is equipped with an optical window allowing for in vivo
125 monitoring of biofilm development on the electrodes using optical coherence tomography
126 (OCT). The 10-liter membrane-less system operates in either anodic (as a microbial
127 electrolysis cell) or cathodic mode with an effective working electrode area of up to 1 m^2
128 (depending on the number of graphite disks mounted). As a proof of principle for an axenic,
129 aerobic MES-process we cultivated *K. spormannii* in the system and correlated the OCT-
130 derived, spacial resolved biovolume of the cathodic biofilm with the radius of the rotating
131 cathodes. Furthermore, we demonstrated that the developed system can also be operated as
132 a microbial electrolysis cell by culturing a co-culture of *Shewanella oneidensis* and *Geobacter*
133 *sulfurreducens* as an anodic biofilm in the RDBER. Thus, we were not only able to demonstrate
134 the general functionality of the system, but also to provide a first insight into the range of
135 possible applications that the RDBER offers as a technological platform for METs.

136

137 **2. Material and methods**

138 **2.1 Reactor Design**

139 The design of the reactor system is illustrated in detail in Fig. 1. The reaction chamber,
140 consisting of the reactor jacket (Fig. 1b) and two flanges, was designed as a horizontal cylinder
141 made of polypropylene. The inner diameter of the jacket measuring 238 mm and the length of
142 230 mm result in an inner volume of the reaction chamber of 10 L. An inspection window made
143 of polycarbonate (Fig. 1a) was integrated in the front flange allowing the observation of the
144 foremost working electrode (Fig. 1d). A circular recess milled in the center of the window serves
145 as a guide and seat for the shaft bearing (Fig. 1f). Figure 1 III shows a cross-sectional view of
146 the RDBER illustrating the arrangement of the electrodes in the reaction chamber. The shaft,
147 which was made of high-purity titanium and sealed from the environment by a shaft seal, is
148 located concentrically in the reactor. A precisely aligned shaft bearing in the rear flange,
149 together with the fixed bearing in the front window, ensures that the shaft runs as friction-free
150 and balanced as possible. For compensation of the temperature-related expansion of the shaft
151 relative to the reaction chamber, the bearing in the rear flange was designed as a floating
152 bearing. The shaft was manufactured as a threaded rod onto which working electrode holders
153 (custom made titanium nuts) are mounted. The working electrode discs made of graphite are
154 clamped between two holders in each case and centered in the process. This ensures that the
155 discs are in contact with the shaft and thus also with the voltage source. In total, up to 14
156 working electrode disks with a thickness of 3 mm and a diameter of 210 mm can be mounted

on the shaft. This corresponds to an active working electrode surface (front and back) of up to 1 m^2 and, relative to the reaction chamber volume, a surface-to-volume ratio of 100 m^2 m^{-3}.

Since in RBC-like systems the cross-flow across the biofilm is adjusted by the rotational speed of the rotating substrate (here the working electrode), a high-resolution stepper motor (Fig. 1c) was implemented (Lexium MDrive Motion Control, Schneider Electric) on the rear flange. The employment of such a stepper motor allows, in addition to the load-independent control of the rotational speed, the position-accurate visualization of selected locations on the substrate. Apart from the toothed belt wheel required for this purpose, a double leg carbon brush holder (Fig. 1l) with silver-graphite brushes was attached to the end of the titanium shaft (Fig. 1n). Via this brush holder, electrical contact was made from the potentiostat to the rotating shaft and thus also to the working electrodes. The counter electrodes were made of titanium sheet with an iridium mixed oxide coating (platinode type 177, Umicore) in the form of half-rounds (Fig. 1m) and connected to each other by means of four titanium threaded rods (Fig. 1o). Exactly cut pieces of titanium pipe (Fig. 1p) are mounted between each two anode sheets to provide the desired distance between the working and counter electrodes. The distance between anode and cathode amount to 5.5 mm. A total of up to 15 fixed counter electrode sheets with an active area of approx. 0.5 m^2 can be installed in the reaction chamber in this way. The four titanium threaded rods are led out of the reaction chamber through the rear flange (Fig. 1i) and can thus be connected to the potentiostat. Cable bushings made of polytetrafluoroethylene (PTFE) provide the necessary sealing.

In order to supply the growing biofilm with CO_2-enriched media during cathodic operation, the gas-saturated and pre-tempered culture medium was pumped by means of a gear pump with an autoclavable pump head (REGLO-Z Digital, Z-1830 P, Ismatec) (Fig. 1t) from an optional stainless-steel (Fig. 1r) double jacket container via a compression fitting (Fig. 1e) located in the front flange into the reaction chamber. The medium is then circulated in the overall system via two screw fittings (Fig. 1h, j) located on the rear flange. During operation the volume flow was led via the compression fitting (Fig. 1j) connected to the reference electrode holder containing an Ag/AgCl reference electrode (Fig. 1q) (SE23I, Meinsberg Sensortechnik). The second screw connection (Fig. 1h) served as an outlet for any gas that may have formed and collected in the reaction chamber.

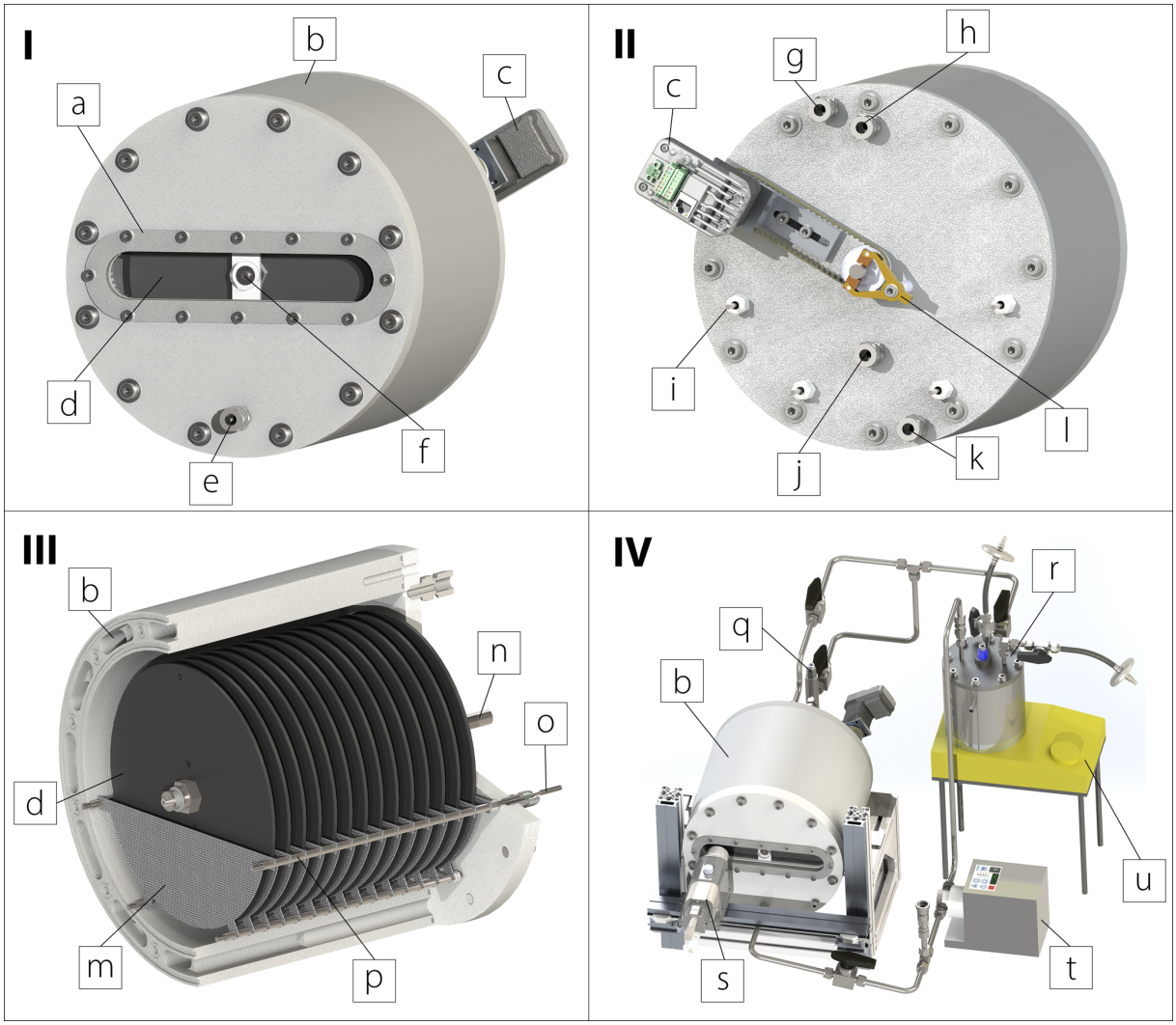

Fig. 1: 3D renderings of the RDBER: (I) Front view of the reaction vessel, (II) rear view of the reaction vessel, (III) cross-section of the reaction vessel, (IV) full system with stainless-steel vessel and piping. (a – inspection window, b – reactor jacket, c – stepper motor , d – working electrode disc, e – inlet to reaction chamber, f – shaft journal bearing, g – outlet of heating jacket, h – gas outlet, i – connector to counter electrode, j – outlet of reaction chamber and connection to reference electrode holder, k – inlet to heating jacket, l – carbon brush holder as connector to rotating working electrodes, m – counter electrodes , n – working electrode shaft , o – counter electrode shaft, p – counter electrode spacers, q – reference electrode, r - double jacketed vessel with integrated pH electrode, s – OCT probe head, t – magnetic gear pump, u – magnetic stirrer).

To ensure constant temperatures in the reaction chamber, heating channels were milled into the 31 mm thick polypropylene jacket. These channels were flushed with heating liquid and are shown in the cross-section of the reaction chamber (Fig. 1 III). Inlet (Fig. 1k) and outlet (Fig. 1g) of the heating jacket were placed at the rear flange of the reaction chamber and coupled to a circulation thermostat via clamping ring connections. Simultaneously the growth medium was heated supportively in the optional stainless-steel double jacket vessel during

204 cathodic operation (Fig. 1r). Moreover, the gaseous substrates for electroautotrophic growth
205 were continuously passed through the headspace of the stainless-steel vessel under pressure.
206 The inlet and outlet of the substrate gases are equipped with sterile filters to prevent
207 contamination. Additional stirring of the medium by means of a magnetic stirrer (Fig. 1u)
208 ensured improved mass transfer of the gases and increased the heat transfer of the heated
209 jacket into the medium. By installing a pH electrode (Ceragel CPS71D, Endress + Hauser) in
210 the vessel, the pH value and temperature was logged and the circulation thermostat was
211 regulated. The RDBER was aligned and rigidly fixed on a base frame. Moreover, a holder on
212 which the OCT probe (Fig. 1f) can be fixed was mounted to the base frame.

213

214 **2.2 Strains and preculture conditions**

215 Electroautotrophic experiments were conducted with a population of *K. spormannii* EA-1^T
216 previously adapted to cathodic growth [16]. The preculture for RDBER experiments was grown
217 from freezer stocks in a modified R2A medium (yeast extract 5 g L^{-1}, tryptone 1 g L^{-1}, casamino
218 acids 0.5 g L^{-1}, sodium pyruvate 0.5 g L^{-1}, $MgSO_4 \cdot 7\ H_2O$ 0.05 g L^{-1}, K_2HPO_4 0.1 g L^{-1}, MOPS
219 10 mM - pH 6) at 60 °C without agitation. The heterotrophically grown pre-culture of
220 *K. spormannii* was washed two times with ES medium (pH 3.5; 10 mM NH_4Cl, 2.5 mM NaCl,
221 0.3 mM KH_2PO_4, 0.12 mM $MgSO_4$, 0.1 mM $CaCl_2$, 1 ml L^{-1} Wolfe's mineral elixir) before
222 inoculating the autoclaved RDBER setup [10]. Depending on the desired planktonic cell
223 number per working electrode surface ratio the initial optical density (OD_{600}) in the RDBER was
224 0.1 or 0.3 respectively. A counting chamber (Bürker-Türk) was consulted in order to determine
225 the specific cell number per OD_{600} and Volume (an OD_{600} of 1 corresponded to 3.16±0.25
226 *K. spormannii* cells per ml).

227 A mixed culture of the model organisms *Shewanella oneidensis* MR-1 and *Geobacter*
228 *sulfurreducens* PCA was employed as biocatalyst during anodic operation of the RDBER.
229 *S. oneidensis* was precultured aerobically in LB-Medium (Lennox), while the cultivation of the
230 *G. sulfurreducens* preculture was conducted under anoxic conditions in BES-Medium
231 [0.42 g L^{-1} KH_2PO_4, 0.22 g L^{-1} K_2HPO_4, 0.2 g L^{-1} NH_4Cl, 0.38 g L^{-1} KCl, 0.36 g L^{-1} NaCl,
232 0.21 g L^{-1} $MgCl_2$, 11.92 g L^{-1} HEPES – after autoclaving the medium was complemented with
233 1 ml L^{-1} 0.4 mM $CaCl_2$ solution, 10 ml L^{-1} NB trace mineral solution, 1.0 ml selenite–tungstate
234 solution (13 mM NaOH, 17 µM Na_2SeO_3, and 12 µM Na_2WO_4), 10 ml vitamin solution (German
235 Type Culture Collection, DSMZ, media 141) and then sparged in rubber sealed bottles with
236 N_2/CO_2 (80:20 vol%) for 30 minutes]. For preculturing, the BES-medium was complemented
237 with 20 mM sodium acetate as electron donor and disodium fumarate (40 mM) as electron
238 acceptor. The final pH was set to 7.4. Before inoculating the reactor with a mixture of

239 *G. sulfurreducens* and *S. oneidensis* in a 9 to 1 ratio to an initial OD_{600} of 0.1, the cells were
240 washed two times in BES-Medium.

241

242 **2.3 Cathodic operation of RDBER**

243 After pumping the previously inoculated ES-Medium into the sterile RDBER, the medium
244 temperature was adjusted to 60 °C. The headspace of the mixing vessel was pressurized to
245 0.5 bar and continuously flushed with a mixture of 99.5% CO_2 (v/v) and 0.5% O_2 (v/v) while the
246 liquid phase was continuously stirred at 300 rpm. The cultivation medium enriched with the
247 gaseous substrates was pumped through the RDBER at a constant volumetric flow rate of
248 500 ml min^{-1}. In order to achieve different planktonic cell number per working electrode surface
249 ratios, either only one or all electrodes were mounted (714 cm^2 vs. 1 m^2 working electrode
250 surface). The rotational speed of the working electrodes amounted to one revolution per
251 minute. A constant current density of 1 µA cm^{-2} was applied for 24 h immediately after
252 inoculation by means of a potentiostat (Interface 5000P, Gamry Instruments, Warmister, USA).
253 After this initial polarization phase, the current density was set to 3 µA cm^{-2} by the end of the
254 experiment. The experiments were stopped upon detection of no further biofilm increase.
255

256 **2.4 Anodic operation of RDBER**

257 10 L of inoculated BES-medium containing 20 mM sodium acetate and 20 mM sodium lactate
258 as carbon source was pumped in the previously autoclaved RDBER. Chronoamperometric
259 batch experiments were performed at 30 °C and a constant working electrode potential of 0 mV
260 vs. SHE (standard hydrogen electrode) was set. For anodic operation the stainless-steel
261 mixing vessel was omitted while the pipeline was shorted with a pH-electrode holder. Evolving
262 reaction gases (e.g. Hydrogen and CO_2) were collected at the upper outlet (Fig. 1h) and led
263 through a MilliGascounter (Ritter, Germany) into a gas sampling bag. Analysis of collected
264 gases was conducted by means of a Micro GC (490 Micro GC, Agilent Technologies,
265 Germany) using two different carrier gases (argon and helium) and two stationary phases (CP-
266 Molsieve 5 Å Plot and PoraPLOT U J&W GC columns, Agilent Technologies, Germany).
267 Moreover, liquid samples were taken twice a day in order to quantify the concentration of
268 organic acids by means of a Metrohm 881 Compact Pro Ion Exchange Chromatograph with a
269 Metrosep Organic Acids 250/7.8 column (Metrohm, Switzerland).

270

271 **2.5 OCT imaging and digital image processing**

272 A GANYMEDE II spectral domain OCT system (Thorlabs GmbH, Dachau, Germany) equipped
273 with a LSM04 objective lens was employed for 3D biofilm visualization (Thorlabs GmbH,

Dachau, Germany). Prior to each OCT acquisition, the stepper motor was consistently halted in the same pre-assigned position. Together with the fixed position of the OCT probe holder, this allowed reproducible visualization of a selected radial cathode section. OCT 3D data sets (C-scans) were acquired regularly over the visualizable radial area (see Fig. 2). Each spot was scanned with a size of 10.0 mm × 6.0 mm × 2.0 mm (L × W × H) and pixel resolutions of 8 µm px^{-1} (lateral, xy-plane) and 2.06 µm px^{-1} (axial, z-direction). Adjacent OCT data sets were then stitched to depict the whole radius of the cathode. The generated OCT datasets were then analyzed, merged, and finally assembled into a height profile (6 mm × 70 mm; H × W). The visualized rectangular area was then trimmed into an isosceles trapezoid for final evaluation. The trapezoid represents a circular sector of the round disk, which abuts the outer radius of the substrate and was shortened to 70 mm by cutting off the tip. 110 of these trapezoids could thus be approximately combined to form a circular ring with an outer diameter of 21 mm and an inner diameter of 70 mm. Finally, the mean biovolume $\overline{BV}$, the mean accumulation rate $\overline{BV}^*$, and the mean coverage $\overline{SC}$ over the radius were determined from the cropped trapezoid (detailed view Figure 2). In addition, the trapezoid was divided into 7 further 10 mm long sub-trapezoids to obtain detailed information about the spatial distribution of biovolume (BV) along the radius of the circular blank. ImageJ [23], operated with in-house made macros [24], was used to calculate topographic representations of the bulk-biofilm interface (height maps) and the structural parameters used for biofilm characterization.

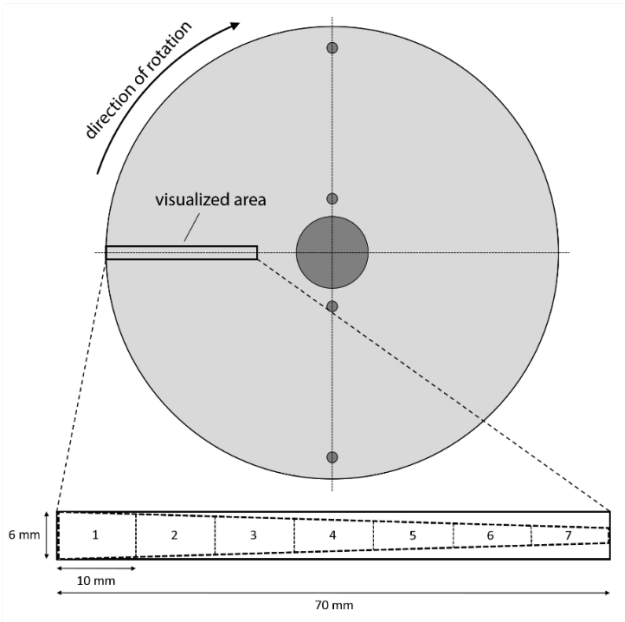

Fig. 2: Representation of the visualized area and the analyzed trapezoidal sections of the generated OCT data sets.

2.6 Parameters for biofilm characterization

The calculation of the biofilm structure parameters - biovolume BV (µm^3 µm^{-2}), mean biovolume $\overline{BV}$ (µm^3 µm^{-2}), mean biofilm accumulation rate $\overline{BV}^*$ (µm^3 µm^{-2} d^{-1}) and mean substratum coverage $\overline{SC}$ (-) was based on height maps according to Wagner and Horn[35].

Biovolume BV is defined as the measured biofilm volume V_{BF} (µm^3) per specific area of a single small trapezoid A_{ST} (µm^2)

$$BV = \frac{V_{BF}}{A_{ST}}$$

whereas $\overline{BV}$ is being defined as

$$\overline{BV} = \frac{\sum V_{BFn}}{\sum A_{STn}}$$

Where n indexes the individual small trapezoids.

Mean biofilm accumulation rate $\overline{BV}^*$ corresponds to $\overline{BV}$ derived by time:

$$\overline{BV}^* = \frac{\partial \overline{BV}}{\partial t}$$

Finally, mean substratum coverage $\overline{SC}$ is described as

$$\overline{SC} = \frac{\sum A_{STn} - A_{uc}}{\sum A_{STn}}$$

with the area of uncovered substratum A_{uc} (biofilm thickness = 0 µm).

3. Results and discussion

3.1 Cultivation of cathodic *K. spormannii* biofilms

In order to prove the functionality of the newly developed reactor concept, two different pure culture cultivations of electroactive microorganisms were performed in the RDBER. Moreover, initial cultivation experiments performed with *K. spormannii* were designed to answer the question of whether an RDC-like reactor could even be a potential technological platform for upscaling a biofilm-based, aerobic MES process that was previously demonstrated in small-scale, custom-made flow cells [12,16]. Thus, as many process parameters as possible were transferred from the established flow cell cultivation to the cultivation of *K. spormannii* in the RDBER (see Table 1). Hence, for preliminary cultivation experiments the previously autoclaved RDBER was filled with sterile ES-Medium (pH 3.5), omitting any organic carbon source and inoculated with *K. spormannii* to an initial OD_{600} of 0.1. The system was then pressurized to 0.5 bars with the substrate gases CO_2 and O_2 and the mediums temperature was set to 60 °C. The rotational speed of the cathodes amounted to 1 rpm. After several days of reactor operation, OCT analysis of the cathode revealed isolated tower-like structures formed on the cathode. However, their quantity and height decreased sharply again in the course of a few days (see Supplementary Fig. 1). Moreover, the surface coverage of the substratum never exceeded 20% even after one month of cultivation. In summary, no continuous biofilm could be detected on the cathodes by OCT during the preliminary cultivations. When examined more closely, there were two particular process parameters that deviated from the flow cell experiments due to the entirely divergent reactor concept of the RDBER: Firstly, the initial cell number per cathode area, and secondly, the hydraulic retention time in the reaction chamber (0.5 min in the flow-cells compared to 18.4 min in the RDBER). However, since in an RBC-like reactor the flow velocity over the substratum depends on the angular velocity of the substrate rather than the hydraulic residence time (HRT), we assumed that HRT was not likely to be the key process parameter that hindered biofilm growth during the preliminary cultivation experiments. In particular, because care was taken to ensure that the angular velocity of the circular blank at the outermost radius should not exceed the optimum flow velocity for cultivation of *K. spormannii* in the flow cell system. Using the circumference of the circular blanks, it was calculated that a velocity of 11 mm s^{-1} is achieved at the outermost radius at a rotational speed of 1 U min^{-1}, which is within the range of the flow velocity over the cathode in the flow cell system based on the previously conducted CFD simulation [12]. Hence, we hypothesized, that the 44 times lower initial cell number per cathode surface ratio ($3.4 * 10^9$ cm^{-2} in the flow-cells vs. $7.6 * 10^7$ cm^{-2} for the preliminary RDBER experiments) might be the limiting factor for consistent biofilm growth.

357 Table 1: Listing of important process parameters comparing the RDBER cultivations of *K. spormannii*
358 performed in this study and flow cell cultivations performed in another study. LSV – Linear sweep
359 voltammetry, CA – Chronoamperometry.

Process parameter	Flow-cell cultivation [18]	Preliminary cultivation (this study)	Optimized cultivation (this study)
Medium	ES-medium	Es-medium	Es-medium
pH	3.5	3.5	3.5
Gas mixture	CO_2/O_2 (99.5:0.5)	CO_2/O_2 (99.5:0.5)	CO_2/O_2 (99.5:0.5)
Pressure	1.5 bar	0.5 bar	0.5 bar
Temperature	60 °C	60 °C	60 °C
Circulation pump speed	100 ml min^{-1}	500 ml min^{-1}	500 ml min^{-1}
Volume $_{reaction\ chamber}$	50 ml	8500 ml	9850 ml
Hydraulic retention time	0.5 min	17 min	19.7 min
Flow velocity / angular velocity over / of substratum at r = 210 mm	up to 21 mm s^{-1}	up to 11 mm s^{-1}	up to 11 mm s^{-1}
Electroanalytics	potentiostatic LSV (first 24 h), then CA (-500 mV vs. SHE)	potentiostatic LSV (first 24 h), then CA (-500 mV vs. SHE)	galvanostatic 1 µA cm^{-2} (first 24 h), then 3 µA cm^{-2}
Volume $_{system}$ (incl. pipes, etc.)	850 ml	9500 ml	10850 ml
Initial OD_{600}	0.1	0.1	0.3
Working Electrode Surface	20 cm^2	10000 cm^2	700 cm^2
Initial cell number per working electrode ratio	1.34 * 10^9 cm^{-2}	3.0 * 10^7 cm^{-2}	1.47 * 10^9 cm^{-2}

360

361 Previously it was shown that at the initially uncovered cathode a part of the dissolved oxygen
362 might be abiotically reduced into reactive oxygen species [12,16]. As the initial cell number
363 decreases, the cumulative ROS-detoxification capacity of the cells also decreases, possibly
364 preventing a sufficient initial cathode coverage that serves as an insulator to minimize abiotic
365 ROS formation. Therefore, we adjusted the cell number to cathode surface ratio for the
366 subsequent experiments. Besides increasing the initial OD_{600} from 0.1 to 0.3, we also reduced
367 the working electrode area to 700 cm^2, in order to avoid the need of a tremendous amount of
368 preculture, which would not have been cultivatable in our laboratory infrastructure yet.
369 Furthermore, the current density of the system was limited by galvanometry to 1 µA cm^{-2} for
370 24 h (and then to 3 µA cm^{-2} for the rest of the experiment) to minimize initial ROS-formation.
371 Operation of the RDBER under adapted process conditions now resulted in the formation of
372 nearly continuous *K. spormannii* biofilms covering more than 90% of the cathode. Figure 3
373 shows a timeseries of height maps derived from OCT datasets covering a radial excerpt of the
374 working electrode.

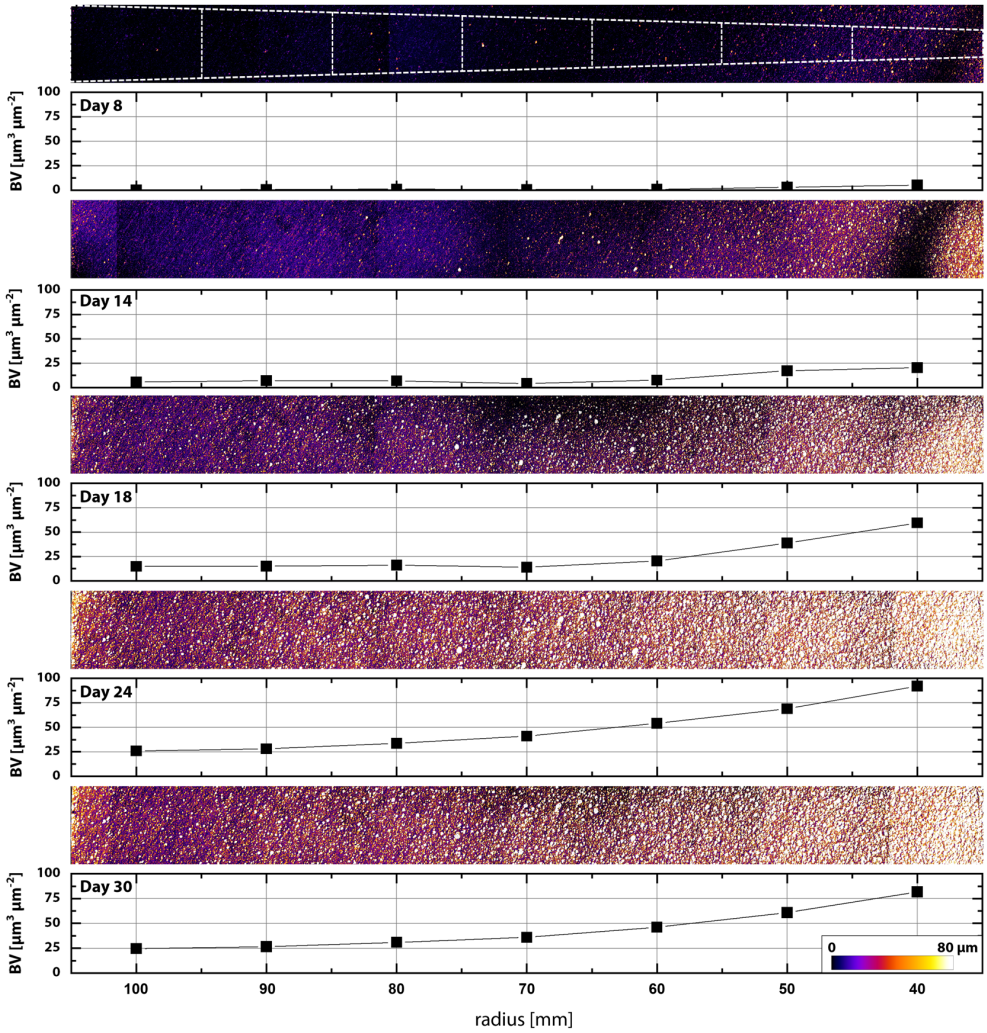

Fig. 3: Time series of selected OCT-derived height maps of the optimized cultivation of *K. spormannii* in the 10 L-RDBER. The same radial section has been visualized on the working electrode in each case in order to show the spatial distribution of the biofilm along the rotating working electrode. Colors are coded from black (0 mm) to white (80 µm). The calculated biovolumes (BV) of the subtrapezoids are shown below the height profiles.

The first visible biofilm structures formed after a lag phase of 8 days near the shaft, i.e. at regions with comparatively low shear stress. A spatially resolved calculation of the local biovolume clearly shows that BV decreases with larger radius towards the edge of the circular blank. So, with an increased angular velocity of the substratum and therefore a higher flow velocity over the biofilm, the biovolume of the *K. spormannii* biofilm is decreasing. After 24 days BV reached the maximum values measured in the course of the experiment in all segments. The maximum BV in the outer region of the cathode averaged 25 $\mu m^3\ \mu m^{-2}$, only about a quarter of the max BV of approximately 100 $\mu m^3\ \mu m^{-2}$ observed in the inner visualized region. The extent to which the biovolume can be used to draw conclusions about the productivity (i.e.,

390 CO_2-fixation rate) of the *K. spormannii* biofilm is not conclusive from this data. Nevertheless, it
391 is known that compressed and denser biofilms generally exhibit higher turnover rates, since
392 more catalytically active biomass is present per biovolume. At the same time, denser biofilm
393 structures might hamper the diffusion of substrates and products within the biofilm [36,37],
394 whereas the heterogeneity of the biofilm structure will also influence diffusion reaction [38].
395 Certainly, the increased shear force at increased angular velocity affects the biofilm height to
396 some extent as well. This effect may also be exploited in a future biotechnological process.
397 Thus, a fluctuating and short-term increase of the rotational speed could serve for an optimal
398 harvesting of the biomass from the substratum. In this way, the planktonic biomass could be
399 partially and discontinuously extracted from the reactor, creating a self-sustaining system,
400 since some of the detached cells can recolonize uncovered areas of the substratum. In order
401 to compare the results of the RDBER system with those of the previously published flow cell
402 experiments, calculated $\overline{BV}$ values were fitted by a logistic growth function:

403 $\overline{BV} = 40.718 + (3.055 - 40.718) / (1 + (t / 17.765)^{11.14})$ ($R^2 = 0.98$)

404 The course of the plotted values of $\overline{BV}$ shows a significantly longer lag phase compared to the
405 flow cell experiments. The highest biofilm accumulation rate of 6 $\mu m^3\ \mu m^{-2}\ d^{-1}$ was reached
406 between days 17 and 18 and was 45% lower compared to the flow cell experiments (see figure
407 6 in [12]). Moreover, the maximal achieved mean biovolume in the RDBER system was
408 42 $\mu m^3\ \mu m^{-2}$, which accounted to around 25% of the max. mean biovolume in the flow-cells.
409 The highest coverage of 87% was reached on day 24, with $\overline{SC}$ not describing a steeply
410 increasing degressive course like in the flow-cell experiments, but a linear course until the
411 biofilm finally detached. The biofilm in the RDBER system thus showed a generally weaker
412 and slower growth per area of cathode surface. Notwithstanding, to our knowledge, this data
413 shows the first successful cultivation of an aerobic, electroautotrophic organism in a BES at
414 this scale (700 cm^{-2} working electrode). One of the reasons for the comparatively slow growth
415 of *K. spormannii* in the RDBER was probably the moderate, limited current density (3 $\mu A\ cm^{-2}$)
416 - especially in contrast to the measured currents of the flow cell experiments (between 13 and
417 20 $\mu A\ cm^{-2}$ at a constant working electrode potential of -500 mV vs. SHE). Although excessive
418 ROS production does not occur if the current density is too low, the biocatalyst may not have
419 enough electrons available for rapid and, above all, complete coverage of the substrate. Thus,
420 in future experiments, the maximum current density should be limited to that extent only during
421 the initial start-up phase and should also be increased as the surface coverage increases.

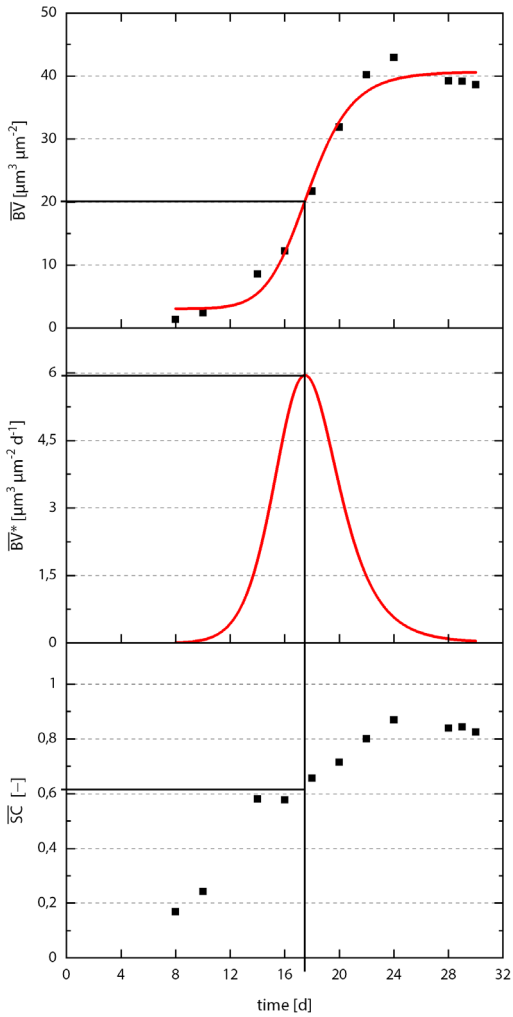

Fig. 4: Plot of calculated biofilm parameters of the optimized cathodic operation of the RDBER over time [mean biovolume ($\overline{BV}$), mean biofilm accumulation rate ($\overline{BV}^*$), and mean substrate coverage ($\overline{SC}$)].

In addition to the limitation of the electron donor, reduced substrate availability due to lower solubility of the gaseous substrates at reduced pressure in the RDBER (0.5 bar) compared to the flow cells (1.5 bar) has to be assumed. Indeed, in their computational model of a microbial electrosynthesis process, Cabau-Peinado et al. demonstrated that CO_2 limitations can occur and thus may play a role in low turnover rates of a MES system [39]. According to the manufacturer, the shaft seal of the titanium shaft in the rear flange is currently the only tender spot that limits the maximum pressure in the system to 0.5 bar. Both the reactor periphery and the entire reactor jacket can be pressurized to at least 1.5 bar. Therefore, future reactor generations should incorporate a shaft seal in the rear bearing that is designed for higher pressure ranges in order to assess the impact of the pressure on the biofilm development in the RDBER.

438 **3.2 Anodic operation as Microbial Electrolysis Cell**

439 Following the successful cultivation of an electroautotrophic species in the RDBER, we used
440 the reactor to cultivate a defined coculture of *Shewanella oneidensis* and *Geobacter*
441 *sulfurreducens*. Both organisms are well-studied electroactive model organisms for
442 extracellular electron transfer of respiratory electrons to insoluble electron acceptors such as
443 an anode of a BES. The anodic operation of the RDBER as a microbial electrolysis cell (MEC)
444 was intended not only to prove the basic functionality of the system, but also to emphasize the
445 flexibility regarding the possible applications of the RDBER. In a MEC, electroactive organisms
446 oxidize organic matter into CO_2 and protons, whereby the released electrons are transferred
447 from the organisms to the anode, which serves as a terminal respiratory electron acceptor.
448 From the anode, the electrons are transferred to the cathode by means of a current source.
449 Subsequently, protons are then reduced to hydrogen at the cathode. The experiments were
450 performed as batch experiments with a full set of the 14 working electrodes (here anodes) with
451 a total surface area of 1 m^2 at a rotational speed of 1 rpm. Acetate and lactate served as carbon
452 source with an initial concentration of 20 mM each. The current density at a constant working
453 electrode potential of 0 mV vs. SHE was recorded over the experimental course of roughly
454 9 days (see Fig 5). After an initial polarization phase of a few hours, characterized by negative
455 current densities most likely due to the depletion of residual oxygen in the system, the current
456 steadily increased until it peaked at 130 µA cm^{-2} after about 4 days. Subsequently, the current
457 density drops again to slowly decrease to about 90 µA cm^{-2} after 9 days. Almost uniform in
458 shape runs the graph of the gas evolution rate recorded by means of a MilliGascounter from
459 the gas outlet of the RDBER. The hydrogen fraction in the outflowing gas was examined
460 regularly using a MicroGC and remained almost constant over the entire experimental period
461 (88.1 ± 1.2%). Daily liquid sampling of the reactor's broth was conducted to determine the
462 concentration of the organic acids via ion chromatography.

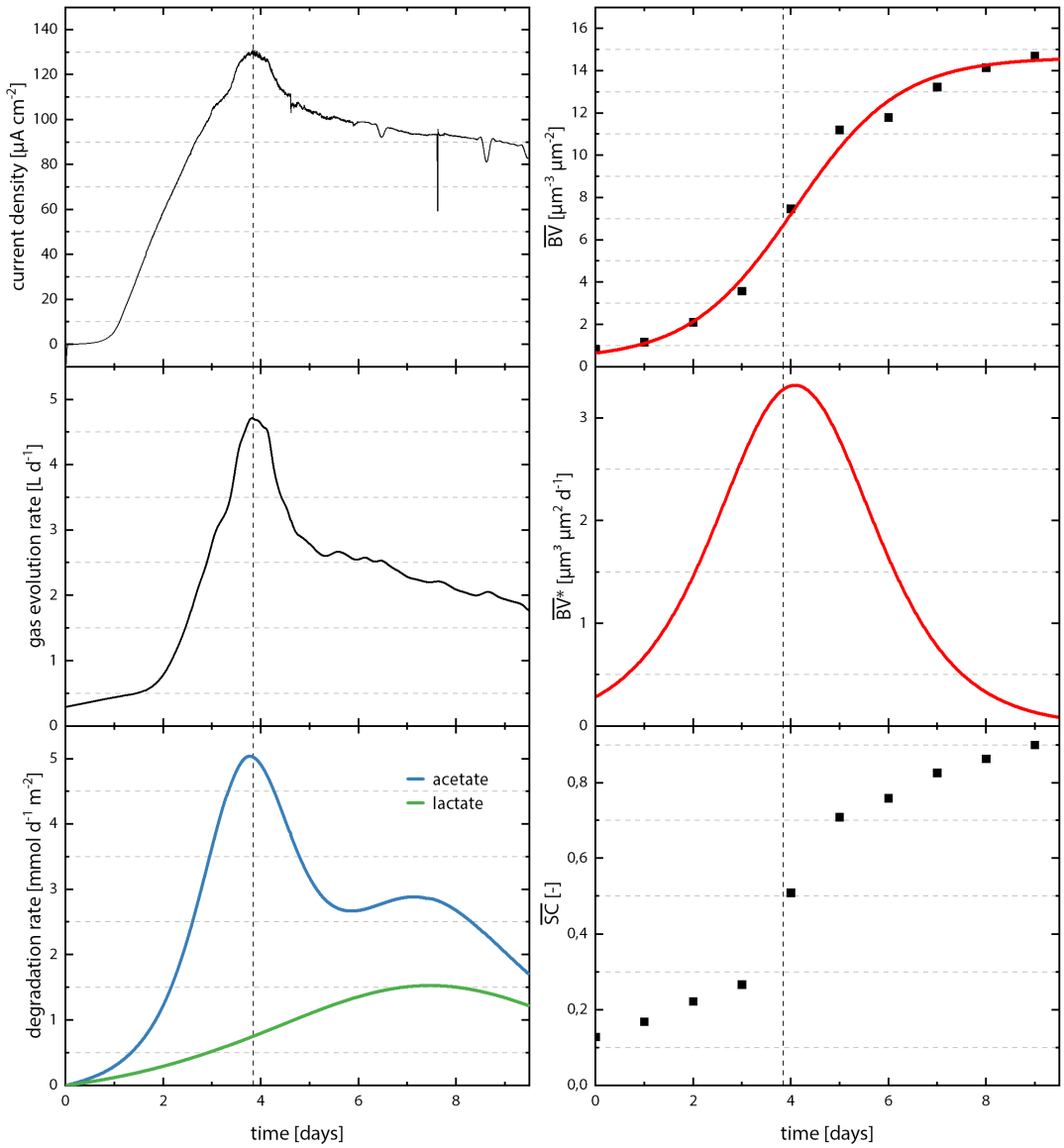

Fig. 5: Correlation of current density, gas evolution rate and substrate specific degradation rate with calculated biofilm parameters obtained during anodic operation of the RDBER. A coculture of *Shewanella oneidensis* and *Geobacter sulfurreducens* was cultivated at a working electrode potential of 0 mV vs. SHE in a MEC-like operation. For a clearer representation, the graphs of current density and gas evolution rate were smoothed with an FFT filter. Raw data of organic acid concentrations, as well as the applied fits (displayed in color), are provided in the Supplementary Material.

The course of the concentration values over time was fitted and derived after time to obtain the specific degradation rates for acetate and lactate, respectively (please refer to the supplementary material for original data and fit). In this context, it was important to consider that *Shewanella* degrades one molecule of lactate into one molecule of acetate and CO_2 or formate. Since the acetate concentration did not increase during the experiment, it was therefore assumed that the acetate produced by *Shewanella* was directly metabolized by

Geobacter. This was taken into account when calculating the specific acetate degradation rate. Since both the peak in current data, and in the gas production rate, correlate with the peak in acetate degradation rate on day 4, these data clearly demonstrate that *Geobacter* is accounting for most of the current production, as *Shewanella* is not capable of metabolizing acetate. The maximum degradation rate for acetate was 5 mmol d^{-1} m^{-2} cathode surface and 1.5 mmol d^{-1} m^{-2} for lactate, respectively. Regular OCT scans of a radial anode section provided the basis for calculating $\overline{BV}$ and $\overline{SC}$. Figure 5 shows the mean biofilm accumulation rate ($\overline{BV}^*$) derived from a logarithmic fit through the calculated $\overline{BV}$ values:

$\overline{BV}$ = 0.343 + (14.646 - 0.343) / (1 + 10^((4.083 - t) * (0.404))) (R^2 = 0.99)

The highest biofilm accumulation rate of almost 3 μm^3 μm^{-2} d^{-1} is likewise reached after about 4 days. Again, based on the correlations with the degradation rate, conclusions can be drawn that *Geobacter* cells appear to be the predominant species in the biofilm. This is also consistent with the literature findings that attribute rather modest biofilm capabilities to *Shewanella* compared to *Geobacter* [40]. After 9 days the anodic biofilm covered around 90% of the observed working electrode surface. Interestingly, the mean surface coverage does not increase linearly as in the cathodic cultivation experiments of *K. spormannii*, but rather logarithmically. Hence, it can be concluded that the growth pattern seen in the cathodic experiments is not so much an intrinsic phenomenon of the RDBER, but probably due to the abiotic formation of ROS on uncovered cathodes described above. Comparing the performance of the RDBER with other single-chamber upscaling attempts of MECs, it is apparent on the one hand that there is still room for improvement in terms of current densities, but on the other hand the excellent surface to reactor volume ratio (100 m^2 m^{-3}) of the RDBER is worth emphasizing [21]. For example, Brown et al. measured current densities up to 720 µA cm^{-2}, but at a surface to volume ratio of 15 m^2 m^{-3} (0.58 m^2 anode area and 30 L reactor volume) [41]. In another study, the measured maximum current densities were in similar ranges around 700 µA, but again with a surface to volume ratio five times lower than in the RDBER [42]. However, it should be noted that the experiments conducted here were only short-term batch experiments to validate the functionality of the system. The above studies were conducted in a continuous operating mode for a significantly longer period of time, up to several months, allowing a more productive biofilm to grow on the working electrode over the longer cultivation period. In addition, the ion chromatographic data also indicate that the biofilm may have already reached a degree of substrate limitation (original data in supplementary material). Furthermore, the optimal rotational speed of the working electrodes must be identified for each future application of the RDBER and thus for each specific microbial community specifically.

4. Conclusions

In conclusion, the study aimed on the design of a novel, scalable electrochemical reactor concept that meets the requirements of biotechnological pure culture cultivations. During the construction of the single-chamber system, emphasis was laid on a long operating lifetime and low-maintenance operation. The successful cultivation of different electroactive model organisms, both in anodic and cathodic operation, prove on the one hand the basic functionality of the system. On the other hand, we were able to demonstrate that an increase in the working electrode area is not only possible by numbering up individual small reactor systems, as is often the case for METs. If microbial electrochemical technologies are to become truly competitive, a greater range of creative reactor designs that can be scaled up without excessive numbering-up is necessary. A further scale-up of the RDBER is conceivable as well: While the diameter of the electrode discs is limited mainly by the angular velocity at the outer edge, the shaft can be extended (and equipped with more electrodes) until it is unable to statically support its own weight. Moreover, based on this work, we were able to show that an RDC-like reactor is, in principle, a feasible way to upscale the previously flow cell-based cultivation of *K. spormannii* for bioplastic production from electricity and CO_2. Since the pumping power required for successful cultivation of *K. spormannii* in an upscaled flow cell process would presumably render the overall process quickly uneconomical, an RDC-like reactor might be an interesting option to generate HRT independent crossflow velocities across the working electrode. Furthermore, the cultivation experiments of *K. spormannii* in the RDBER highlighted the crucial role of the start-up phase in aerobic MES processes. The impact of reactive oxygen species should not be underestimated in the development of future MES processes. Therefore, for the necessary development of targeted strategies, it is important to better understand the formation of reactive oxygen species at cathodes under physiological conditions, as well as the different detoxification mechanisms of electroautotrophic microorganisms.

5. Funding

This work was supported by a grant of the Federal Ministry of Education and Research (BMBF) as part of the BioElectroPlast project, no. 033RC006.

6. Declaration of Competing Interest

The authors declare that they have no known competing financial interests or personal relationships that could have appeared to influence the work reported in this paper.

7. Acknowledgements

Special thanks go to Prof. Harald Horn for the initial idea behind the reactor concept, to Axel Heidt as the person responsible for the IC measurements and to Erwin Wachter, Joachim Lang and Alfred Herbst from the metal workshop of the EBI for their work and support during the construction of the reactor.

8. References

[1] M. Lieder, A. Rashid, Towards circular economy implementation: A comprehensive review in context of manufacturing industry, J Clean Prod. 115 (2016) 36–51. https://doi.org/10.1016/j.jclepro.2015.12.042.

[2] T. Krieg, L.M.P. Phan, J.A. Wood, A. Sydow, I. Vassilev, J.O. Krömer, K.M. Mangold, D. Holtmann, Characterization of a membrane-separated and a membrane-less electrobioreactor for bioelectrochemical syntheses, Biotechnol Bioeng. 115 (2018) 1705–1716. https://doi.org/10.1002/BIT.26600.

[3] K.P. Nevin, T.L. Woodard, A.E. Franks, Z.M. Summers, D.R. Lovley, Microbial electrosynthesis: Feeding microbes electricity to convert carbon dioxide and water to multicarbon extracellular organic compounds, MBio. 1 (2010) e00103-10. https://doi.org/10.1128/mBio.00103-10.

[4] B.E. Logan, R. Rossi, A. Ragab, P.E. Saikaly, Electroactive microorganisms in bioelectrochemical systems, Nat Rev Microbiol. 17 (2019) 307–319. https://doi.org/10.1038/s41579-019-0173-x.

[5] X. Christodoulou, S.B. Velasquez-Orta, Microbial electrosynthesis and anaerobic fermentation: An economic evaluation for acetic acid production from CO_2 and CO, Environ Sci Technol. (2016) acs.est.6b02101. https://doi.org/10.1021/acs.est.6b02101.

[6] L. Jourdin, T. Burdyny, Microbial Electrosynthesis: Where Do We Go from Here?, Trends Biotechnol. 39 (2021) 359–369. https://doi.org/10.1016/J.TIBTECH.2020.10.014.

[7] L. Jourdin, J. Sousa, N. van Stralen, D.P.B.T.B. Strik, Techno-economic assessment of microbial electrosynthesis from CO_2 and/or organics: An interdisciplinary roadmap towards future research and application, Appl Energy. 279 (2020) 115775. https://doi.org/10.1016/J.APENERGY.2020.115775.

[8] A. Prévoteau, J.M. Carvajal-Arroyo, R. Ganigué, K. Rabaey, Microbial electrosynthesis from CO_2: forever a promise?, Curr Opin Biotechnol. 62 (2020) 48–57. https://doi.org/10.1016/j.copbio.2019.08.014.

[9] J.C. Wood, J. Grové, E. Marcellin, J.K. Heffernan, S. Hu, Z. Yuan, B. Virdis, Strategies to improve viability of a circular carbon bioeconomy-A techno-economic review of microbial

585 electrosynthesis and gas fermentation, Water Res. 201 (2021).
586 https://doi.org/10.1016/J.WATRES.2021.117306.

587 [10] J.E. Reiner, T. Jung, C.J. Lapp, M. Siedler, B. Bunk, J. Overmann, J. Gescher, *Kyrpidia spormannii*
588 sp. nov., a thermophilic, hydrogenoxidizing, facultative autotroph, isolated from hydrothermal
589 systems at São Miguel Island, and emended description of the genus *Kyrpidia*, Int J Syst Evol
590 Microbiol. 68 (2018) 3735–3740. https://doi.org/10.1099/IJSEM.0.003037/CITE/REFWORKS.

591 [11] J.E. Reiner, K. Geiger, M. Hackbarth, M. Fink, C.J. Lapp, T. Jung, A. Dötsch, M. Hügler, M.
592 Wagner, A. Hille-Reichel, W. Wilcke, S. Kerzenmacher, H. Horn, J. Gescher, From an
593 extremophilic community to an electroautotrophic production strain: identifying a novel
594 Knallgas bacterium as cathodic biofilm biocatalyst, ISME J. 14 (2020) 1125–1140.
595 https://doi.org/10.1038/S41396-020-0595-5.

596 [12] M. Hackbarth, T. Jung, J.E. Reiner, J. Gescher, H. Horn, A. Hille-Reichel, M. Wagner, Monitoring
597 and quantification of bioelectrochemical *Kyrpidia spormannii* biofilm development in a novel
598 flow cell setup, Chemical Engineering Journal. 390 (2020) 124604.
599 https://doi.org/10.1016/J.CEJ.2020.124604.

600 [13] I. Vassilev, P. Dessì, S. Puig, M. Kokko, Cathodic biofilms – A prerequisite for microbial
601 electrosynthesis, Bioresour Technol. 348 (2022).
602 https://doi.org/10.1016/j.biortech.2022.126788.

603 [14] P.J. Barham, A. Keller, E.L. Otun, P.A. Holmes, Crystallization and morphology of a bacterial
604 thermoplastic: poly-3-hydroxybutyrate, J Mater Sci. 19 (1984) 2781–2794.
605 https://doi.org/10.1007/BF01026954.

606 [15] G. Pillot, S. Sunny, V. Comes, A. Heussner, S. Kerzenmacher, Effect of cathode properties on
607 the thermophilic electrosynthesis of PolyHydroxyAlkanoates by *Kyrpidia spormannii*,
608 Bioresour Technol Rep. 18 (2022) 101040. https://doi.org/10.1016/J.BITEB.2022.101040.

609 [16] T. Jung, M. Hackbarth, H. Horn, J. Gescher, Improving the Cathodic Biofilm Growth Capabilities
610 of *Kyrpidia spormannii* EA-1 by Undirected Mutagenesis, Microorganisms 2021, Vol. 9, Page
611 77. 9 (2020) 77. https://doi.org/10.3390/MICROORGANISMS9010077.

612 [17] K. Guo, A. Prévoteau, S.A. Patil, K. Rabaey, Engineering electrodes for microbial
613 electrocatalysis, Curr Opin Biotechnol. 33 (2015) 149–156.
614 https://doi.org/10.1016/J.COPBIO.2015.02.014.

615 [18] S. Kerzenmacher, Engineering of Microbial Electrodes, in: Springer, Berlin, Heidelberg, 2017:
616 pp. 1–46. https://doi.org/10.1007/10_2017_16.

617 [19] S. Zhang, J. Jiang, H. Wang, F. Li, T. Hua, W. Wang, A review of microbial electrosynthesis
618 applied to carbon dioxide capture and conversion: The basic principles, electrode materials,
619 and bioproducts, Journal of CO_2 Utilization. 51 (2021).
620 https://doi.org/10.1016/j.jcou.2021.101640.

621 [20] G. Pillot, S. Sunny, V. Comes, S. Kerzenmacher, Optimization of growth and electrosynthesis of
622 PolyHydroxyAlkanoates by the thermophilic bacterium *Kyrpidia spormannii*, Bioresour
623 Technol Rep. 17 (2022) 100949. https://doi.org/10.1016/J.BITEB.2022.100949.

624 [21] F. Enzmann, M. Stöckl, A.-P. Zeng, D. Holtmann, Same but different-Scale up and numbering
625 up in electrobiotechnology and photobiotechnology, (2018).
626 https://doi.org/10.1002/elsc.201800160.

[22] T. Krieg, J. Madjarov, L.F.M. Rosa, F. Enzmann, F. Harnisch, D. Holtmann, K. Rabaey, T. Krieg, F. Enzmann, D. Holtmann, J. Madjarov, L.F.M. Rosa, F. Harnisch, K. Rabaey, Reactors for Microbial Electrobiotechnology, Adv Biochem Eng Biotechnol. 167 (2018) 231–271. https://doi.org/10.1007/10_2017_40.

[23] F. Enzmann, F. Mayer, M. Stöckl, K.M. Mangold, R. Hommel, D. Holtmann, Transferring bioelectrochemical processes from H-cells to a scalable bubble column reactor, Chem Eng Sci. 193 (2019) 133–143. https://doi.org/10.1016/J.CES.2018.08.056.

[24] S. Gildemyn, K. Verbeeck, R. Jansen, K. Rabaey, The type of ion selective membrane determines stability and production levels of microbial electrosynthesis, Bioresour Technol. 224 (2017) 358–364. https://doi.org/10.1016/J.BIORTECH.2016.11.088.

[25] K. Guo, A. Prévoteau, K. Rabaey, A novel tubular microbial electrolysis cell for high rate hydrogen production, J Power Sources. 356 (2017) 484–490. https://doi.org/10.1016/J.JPOWSOUR.2017.03.029.

[26] M. Zeppilli, A. Lai, M. Villano, M. Majone, Anion vs cation exchange membrane strongly affect mechanisms and yield of CO_2 fixation in a microbial electrolysis cell, Chemical Engineering Journal. 304 (2016) 10–19. https://doi.org/10.1016/J.CEJ.2016.06.020.

[27] T. Utesch, A.P. Zeng, A novel All-in-One electrolysis electrode and bioreactor enable better study of electrochemical effects and electricity-aided bioprocesses, Eng Life Sci. 18 (2018) 600. https://doi.org/10.1002/ELSC.201700198.

[28] F. Kracke, B. Lai, S. Yu, J.O. Krömer, Balancing cellular redox metabolism in microbial electrosynthesis and electro fermentation – A chance for metabolic engineering, Metab Eng. 45 (2018) 109–120. https://doi.org/10.1016/j.ymben.2017.12.003.

[29] F. Hassard, J. Biddle, E. Cartmell, B. Jefferson, S. Tyrrel, T. Stephenson, Rotating biological contactors for wastewater treatment – A review, Process Safety and Environmental Protection. 94 (2015) 285–306. https://doi.org/10.1016/J.PSEP.2014.07.003.

[30] S. Cortez, P. Teixeira, R. Oliveira, M. Mota, Rotating biological contactors: A review on main factors affecting performance, Rev Environ Sci Biotechnol. 7 (2008) 155–172. https://doi.org/10.1007/S11157-008-9127-X/TABLES/4.

[31] J. Rodziewicz, A. Mielcarek, W. Janczukowicz, T. Jóźwiak, J. Struk – Sokołowska, K. Bryszewski, The share of electrochemical reduction, hydrogenotrophic and heterotrophic denitrification in nitrogen removal in rotating electrobiological contactor (REBC) treating wastewater from soilless cultivation systems, Science of The Total Environment. 683 (2019) 21–28. https://doi.org/10.1016/J.SCITOTENV.2019.05.239.

[32] R.R. Sayess, P.E. Saikaly, M. El-Fadel, D. Li, L. Semerjian, Reactor performance in terms of COD and nitrogen removal and bacterial community structure of a three-stage rotating bioelectrochemical contactor, Water Res. 47 (2013) 881–894. https://doi.org/10.1016/J.WATRES.2012.11.023.

[33] K.Y. Cheng, G. Ho, R. Cord-Ruwisch, Novel methanogenic rotatable bioelectrochemical system operated with polarity inversion, Environ Sci Technol. 45 (2011) 796–802. https://doi.org/10.1021/ES102482J/SUPPL_FILE/ES102482J_SI_001.PDF.

[34] K.Y. Cheng, G. Ho, R. Cord-Ruwisch, Energy-efficient treatment of organic wastewater streams using a rotatable bioelectrochemical contactor (RBEC), Bioresour Technol. 126 (2012) 431–436. https://doi.org/10.1016/J.BIORTECH.2011.12.011.

[35] M. Wagner, H. Horn, Optical coherence tomography in biofilm research: A comprehensive review, Biotechnol Bioeng. 114 (2017) 1386–1402. https://doi.org/10.1002/BIT.26283.

[36] H. Horn, E. Morgenroth, Transport of oxygen, sodium chloride, and sodium nitrate in biofilms, Chem Eng Sci. 61 (2006) 1347–1356. https://doi.org/10.1016/J.CES.2005.08.027.

[37] D. de Beer, P. Stoodley, F. Roe, Z. Lewandowski, Effects of biofilm structures on oxygen distribution and mass transport, Biotechnol Bioeng. 43 (1994) 1131–1138. https://doi.org/10.1002/BIT.260431118.

[38] L. van den Berg, C.M. Kirkland, J.D. Seymour, S.L. Codd, M.C.M. van Loosdrecht, M.K. de Kreuk, Heterogeneous diffusion in aerobic granular sludge, Biotechnol Bioeng. 117 (2020) 3809. https://doi.org/10.1002/BIT.27522.

[39] O. Cabau-Peinado, A.J.J. Straathof, L. Jourdin, A General Model for Biofilm-Driven Microbial Electrosynthesis of Carboxylates From CO_2, Front Microbiol. 12 (2021) 1405. https://doi.org/10.3389/FMICB.2021.669218/BIBTEX.

[40] C. Engel, F. Schattenberg, K. Dohnt, U. Schröder, S. Müller, R. Krull, Long-Term Behavior of Defined Mixed Cultures of *Geobacter sulfurreducens* and *Shewanella oneidensis* in Bioelectrochemical Systems, Front Bioeng Biotechnol. 7 (2019). https://doi.org/10.3389/FBIOE.2019.00060.

[41] R.K. Brown, F. Harnisch, S. Wirth, H. Wahlandt, T. Dockhorn, N. Dichtl, U. Schröder, Evaluating the effects of scaling up on the performance of bioelectrochemical systems using a technical scale microbial electrolysis cell, Bioresour Technol. 163 (2014) 206–213. https://doi.org/10.1016/J.BIORTECH.2014.04.044.

[42] R.D. Cusick, B. Bryan, D.S. Parker, M.D. Merrill, M. Mehanna, P.D. Kiely, G. Liu, B.E. Logan, Performance of a pilot-scale continuous flow microbial electrolysis cell fed winery wastewater, Appl Microbiol Biotechnol. 89 (2011) 2053–2063. https://doi.org/10.1007/S00253-011-3130-9.